AIP Publishing

This manuscript was accepted by Phys. Plasmas. Click here to see the version of record.

Dynamic structure factor of strongly coupled Yukawa plasmas with dissipation

Hanno Kählert[1]
Christian-Albrechts-Universität zu Kiel, Institut für Theoretische Physik und Astrophysik, Leibnizstr. 15, 24098 Kiel, Germany

(Dated: 24 May 2019)

The dynamic structure factor (DSF) of the three-dimensional Yukawa one-component plasma is studied with molecular and Langevin dynamics simulations at moderate and strong coupling. The focus of the investigation is on the dependence of the DSF on the friction coefficient in different frequency and wavenumber regimes. At small to intermediate wavenumbers, frictional damping reduces the strength of the sound peak and leads to a red-shift of its frequency. In an intermediate range of friction coefficients, reducing the wavenumber leads to the vanishing of the sound peak at a finite frequency and the formation of a maximum at zero frequency. This is in contrast to simulations without friction, where the characteristic Rayleigh and Brillouin peaks are observed. The Rayleigh peak around zero frequency for systems without dissipation is generally weak. The simulations show that a small amount of friction can initially decrease its height even further before a strong single maximum is formed at strong damping. At large wavenumbers, the DSF of moderately coupled Yukawa plasmas with dissipation is well described by a single-particle model without interactions, provided frictional damping is taken into account.

I. INTRODUCTION

Strongly coupled plasmas exhibit short-range order and share many similarities with dense liquids. Strong coupling is encountered in a variety of different systems, including warm dense matter (WDM),[1,2] ultracold neutral plasmas (UCNPs),[3] or complex plasmas.[4] WDM states are relevant to inertial confinement fusion[5,6] and can be found in the interiors of giant planets.[7] Here, the electrons are typically moderately coupled and exhibit quantum effects whereas the ions are classical and strongly coupled. Ultracold neutral plasmas[8] are formed after photoionization of confined laser-cooled atoms. Complex plasmas[9] contain, in addition to a background of weakly coupled electrons and ions, highly charged and, therefore, strongly coupled dust particles with sizes of up to a few microns.

The dynamic structure factor (DSF) of the strongly coupled species contains a wealth of information on the plasma state. It is not only affected by the strong coupling of the ions or the dust particles but also by their interaction with the other species. One of the reasons is screening, either induced by electrons (WDM, UCNPs) or by electrons and ions (complex plasmas), which limits the range of the interaction. In addition, (effective) collisions between the different species can influence the DSF. In Ref. 10, this was demonstrated for WDM using Langevin dynamics simulations to mimic effects related to dynamic electron-ion collisions.[11] It was found that a strongly diffusive mode appears in the DSF around zero frequency, in strong contrast to simulations that neglect dissipation. At the same time, the sound speed of the ion-acoustic mode was significantly reduced. The same approach has been used to study the effect of dust-neutral collisions on the longitudinal and transverse collective modes in two-dimensional complex plasmas.[12–16] It has been shown that dissipation not only affects the low-frequency acoustic modes but also the higher harmonics of the magnetoplasmon in magnetized plasmas,[15] which occur at very high frequencies. They were found to successively disappear as the friction coefficient was increased. The effect of frictional damping on wave spectra in strongly coupled plasmas was also investigated with theoretical approaches such as the Quasi-Localized Charge Approximation[17] or harmonic lattice theory.[18] Besides plasmas, dissipation plays a major role in colloidal suspensions.[19–21]

In complex plasmas, the DSF (or closely related quantities such as the longitudinal current fluctuation spectra[14,22]) can be determined directly from the positions of the dust particles. In recent years, sophisticated diagnostics have been developed for the investigation of complex plasmas on the particle level.[23] The DSF of the ions in WDM has been studied in detail with DFT-MD simulations, where electrons are treated with density functional theory (DFT) and ions are propagated classically using molecular dynamics (MD).[10,24–26] Approaches based on pair potentials have also been employed.[27–29] The experimental determination of the ion feature in the DSF of WDM should become feasible with inelastic X-ray scattering.[30]

The goal of the present work is to obtain a comprehensive understanding of the effect of dissipation on the DSF. Since many strongly coupled systems, including the dust particles in complex plasmas or ions in WDM, can often be approximately described by a Coulomb potential with exponential screening (neglecting specific effects such as wake potentials due to streaming ions in complex plasmas[31–33] or additional short-range repulsion due to overlapping electron shells in WDM[27,34]) the focus here is on the 3D Yukawa one-component plasma (YOCP). In particular, for complex plasmas, wake effects become weak at high pressure (high ion-neutral damping),[31,35] i.e., in a regime where dust-neutral collisions become important. The YOCP[36] has been studied extensively, both in 2D[37–39] and in 3D[40–46] and serves as a widely accepted reference system. Dissipation effects are included via the Langevin approach as in previous works.[10,13–15,47] The results presented here are directly relevant to the dust particles in complex plasmas at moderate to high pressure. In addition, they should allow one to make qualitative predictions for systems described by more specialized methods or potentials.

The simulations show that even a small amount of friction can change the DSF significantly. Dissipation reduces the height of the sound peak and shifts the peak position to lower frequencies. While systems without damping feature a well-defined sound mode in the small wavenumber limit, a finite-

ACCEPTED MANUSCRIPT

This manuscript was accepted by Phys. Plasmas. Click here to see the version of record.

AIP Publishing

frequency sound peak can disappear if dissipation is included. Increasing the damping rate leads to the buildup of a maximum in the DSF at zero frequency. In systems with a well-defined Rayleigh peak in the frictionless limit, dissipation can initially reduce the peak height. At large wavenumbers and at moderate coupling, a single-particle model with frictional damping included is able to describe the deviations from the Gaussian shape of the DSF in systems with dissipation.

This paper is organized as follows. The physical model system and the numerical methods are introduced in Sec. II. In Sec. III, the results of the simulations are presented and discussed. Section IV provides a summary of the findings and a brief outlook.

II. MODEL AND SIMULATION METHODS

The Yukawa one-component plasma is composed of N identical particles with mass m and charge q. Their interaction potential is given by

$$v(r) = \frac{q^2}{r}\exp(-r/\lambda), \tag{1}$$

where λ is the screening length. The system has density n and temperature T. Its state is fully specified by the coupling parameter Γ and the screening parameter κ, which are defined in terms of the Wigner-Seitz radius, $a = [3/(4\pi n)]^{1/3}$, as

$$\Gamma = \frac{q^2/a}{k_\mathrm{B}T}, \qquad \kappa = \frac{a}{\lambda}. \tag{2}$$

The Langevin equation of motion for the particle $i \in \{1,\ldots,N\}$ is given by

$$m\ddot{\boldsymbol{r}}_i = \sum_{j\neq i}^{N} \boldsymbol{F}_{ij} - \nu m\dot{\boldsymbol{r}}_i + \boldsymbol{f}_i(t), \tag{3}$$

where $\boldsymbol{F}_{ij}$ is the force of particle j on i, ν the friction coefficient, and $\boldsymbol{f}_i(t)$ a random force term. The latter has zero mean and is related to the friction coefficient via the fluctuation-dissipation theorem, $\langle f_{i\alpha}(t) f_{i\beta}(t')\rangle = 2m\nu k_\mathrm{B}T\,\delta(t-t')\,\delta_{\alpha\beta}\delta_{ij}$. Here, $i,j \in \{1,\ldots,N\}$ are particle indices, and $\alpha,\beta \in \{x,y,z\}$ denote coordinates. For the numerical integration of Eq. (3), the SLO (symplectic low order) algorithm of Ref. 48 is used. In the zero friction limit, the velocity Verlet algorithm is employed instead. For simulations based on the Langevin equation, the third parameter, in addition to κ and Γ, is the value of the reduced friction coefficient, ν/ω_p, where $\omega_\mathrm{p} = \sqrt{3q^2/(ma^3)}$ is the plasma frequency.

The dynamic structure factor $S(\boldsymbol{k},\omega)$ is defined as the Fourier transform of the intermediate scattering function (ISF),[49–51]

$$F(\boldsymbol{k},t) = \frac{1}{N}\langle n(\boldsymbol{k},t)n^*(\boldsymbol{k},0)\rangle, \tag{4}$$

where $n(\boldsymbol{k},t) = \sum_{i=1}^{N} e^{-i\boldsymbol{k}\cdot\boldsymbol{r}_i(t)}$ is the spatial Fourier transform of the microscopic density. In the simulation,[52] the computation of the DSF is based on the relation (see, e.g., Refs. 15, 54–56)

$$S(\boldsymbol{k},\omega) = \lim_{\Delta T\to\infty} \frac{1}{2\pi N}\frac{\langle |n(\boldsymbol{k},\omega)|^2\rangle}{\Delta T}, \tag{5}$$

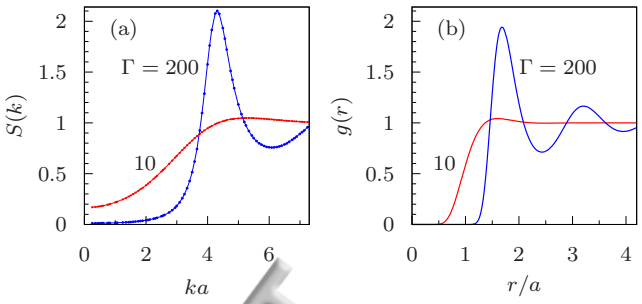

FIG. 1. (a) Static structure factor and (b) pair distribution function for the systems studied in this work with $\kappa = 2$. The coupling parameter Γ is indicated in the figure.

where $n(\boldsymbol{k},\omega)$ is the Fourier transform of $n(\boldsymbol{k},t)$ over a time interval ΔT. In order to improve statistics, $40-120$ simulations of length $27000\,\omega_\mathrm{p}^{-1}$ are performed and subsequently averaged for the same parameters.

III. RESULTS

Simulations have been performed for a screening parameter $\kappa = 2$ with two different coupling strengths, $\Gamma = 10$ and $\Gamma = 200$, covering the moderately and the strongly coupled regime, respectively. The structural properties are illustrated in Fig. 1, which shows the static structure factor, $S(\boldsymbol{k}) = F(\boldsymbol{k},t=0)$, and the pair distribution function, $g(r)$. While the system with $\Gamma = 10$ exhibits a pronounced correlation hole in the pair distribution function, it does not show significant oscillations in $g(r)$, which appear only in the more strongly coupled system with $\Gamma = 200$. The increased structural order also manifests itself in the static structure factor, see Fig. 1(a).

The friction coefficient is varied from $\nu/\omega_\mathrm{p} = 0$ up to $\nu/\omega_\mathrm{p} = 1$, in order to trace the transition from a frictionless to a strongly damped system. The simulations are carried out for $N = 3800$ particles, which results in a minimum wavenumber $k_\mathrm{min} \approx 0.25/a$. This is sufficient to probe the system in a variety of different regimes, including long wavelengths.

III.1. DSF with dissipation

The effect of the friction coefficient on the DSF for various different wavenumbers is illustrated in Fig. 2 for a coupling strength $\Gamma = 10$. In the system without friction, the DSF shows a well pronounced sound peak and a much smaller zero frequency peak for the smallest wavenumber, $ka = 0.433$ [Fig. 2(a)]. At $ka = 0.999$, the local maximum at $\omega = 0$ has almost vanished, and the sound peak has become significantly broader. As the wavenumber increases further, the DSF forms a valley in the low frequency region without a maximum at $\omega = 0$ [Fig. 2(c)], which eventually transforms into a broad plateau, and the DSF decays monotonically [Fig. 2(d)]. This behavior is consistent with earlier observations for strongly coupled Yukawa plasmas.[41,57]

ACCEPTED MANUSCRIPT

This manuscript was accepted by Phys. Plasmas. Click here to see the version of record.

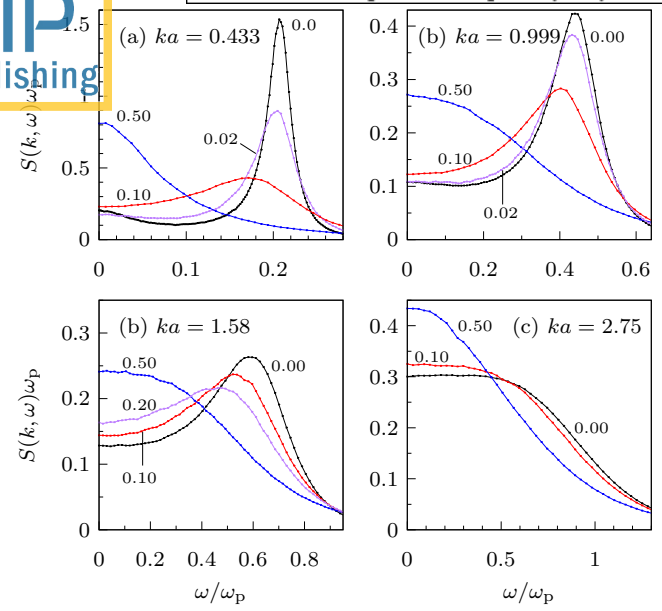

FIG. 2. Dynamic structure factor $S(k,\omega)$ for a system with $\kappa = 2$ and $\Gamma = 10$ as a function of frequency for different wavenumbers ka. The numbers in the figure denote the value of the friction coefficient, ν/ω_p.

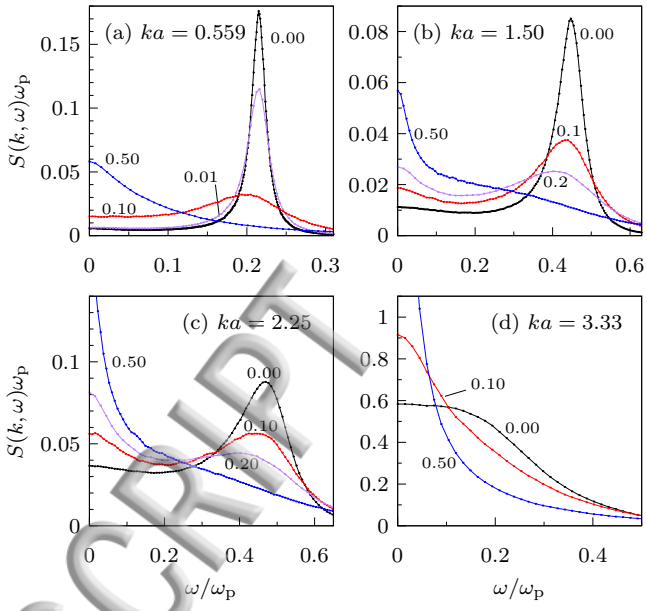

FIG. 3. Dynamic structure factor $S(k,\omega)$ for a system with $\kappa = 2$ and $\Gamma = 200$ as a function of frequency for different wavenumbers ka. The numbers in the figure denote the value of the friction coefficient, ν/ω_p.

The effect of friction is twofold. Provided a well-pronounced sound peak exists for $\nu = 0$, a small damping rate leads (i) to a reduction of the peak height and (ii) shifts the peak position to lower frequencies, see Fig. 2(a) and Fig. 2(b). At the same time, the DSF is modified substantially in the low-frequency domain. At the smallest wavenumber, $ka = 0.433$, damping initially leads to a slight reduction of the maximum at $\omega = 0$, compare $\nu/\omega_p = 0$ and $\nu/\omega_p = 0.02$. As the damping becomes stronger, the DSF increases in this region. This non-monotonic behavior will be investigated more closely in Sec. III.2. At $ka = 0.999$, the zero frequency maximum for $\nu = 0$ is much weaker, and an initial decrease for finite damping is not observed but might possibly occur for even lower values of the friction coefficient. For strong damping, the DSF has its maximum at $\omega = 0$, and the peak at finite frequency vanishes. At larger values of the wavenumber, see Fig. 2(c) and (d), the effect is very similar. The vanishing of the maximum at finite frequencies and the emergence of the zero frequency peak are analogous to previous simulation results for ions in warm dense matter.[10]

Consider now the case $\Gamma = 200$ in Fig. 3. In the system without friction, the simulations show a well-pronounced sound mode at $ka = 0.559$ and $ka = 1.50$. It has been shown that in Yukawa plasmas, the thermal Rayleigh mode around zero frequency is typically weak, in particular at very strong coupling. The reason is that the ratio of specific heats, which controls the relative intensities of the Rayleigh and Brillouin (sound) peaks at small k,[51] is very close to 1.[41,57] This is also observed here, see Fig. 3(a), where the local maximum at $\omega = 0$ is barely noticeable. As the wavenumber increases, the sound peak broadens and finally vanishes [Fig. 3(d)]. Similar to the case $\Gamma = 10$, the DSF decays monotonically for large wavenumbers, with a maximum at $\omega = 0$.

For small wavenumbers, the observations for the damped system are also similar to the case $\Gamma = 10$, see Fig. 3(a). Damping leads to a reduction and a red-shift of the sound peak. At the same time, the DSF increases at zero frequency, which gives rise to a monotonically decaying DSF at large damping ($\nu/\omega_p = 0.5$). For intermediate wavenumbers, on the other hand, the observations are somewhat different, see Fig. 3(b) and Fig. 3(c). Here, damping initially leads to the emergence of a well-defined two-peak structure for $\nu/\omega_p = 0.1$ and $\nu/\omega_p = 0.2$, which is significantly more pronounced than for $\nu/\omega_p = 0$. Here, spectral weight is transferred from the sound peak to the peak at $\omega = 0$. At even higher damping, the remnant of the sound peak disappears, and the DSF develops a very narrow peak around zero frequency, which is followed by a much slower decay of the DSF towards larger frequencies, see $\nu/\omega_p = 0.5$. At the highest wavenumber, shown in Fig. 3(d), the width of the DSF significantly reduces as the friction coefficient is increased.

III.2. Small wavenumber regime

The hydrodynamic limit of the DSF for the Yukawa OCP without dissipation has been studied in Ref. 41, and the criterion for the hydrodynamic description to apply has been determined as $ka < 0.43\,\kappa$. This condition is satisfied for the smallest wavenumbers used here with $ka \gtrsim 0.25$ and $\kappa = 2$. In this section, the effect of friction on the small wavenumber and low frequency limit of the DSF is investigated in more detail.

Figures 4 and 5 show the DSF for small wavenumbers in systems with and without dissipation. In the frictionless case, the sound peak becomes significantly more narrow as

ACCEPTED MANUSCRIPT

This manuscript was accepted by Phys. Plasmas. Click here to see the version of record.

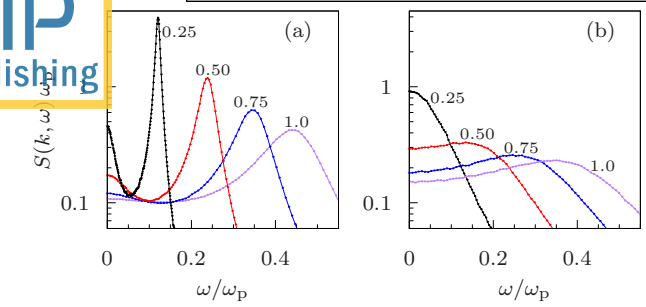

FIG. 4. Dynamic structure factor for a system with screening parameter $\kappa = 2$ and coupling parameter $\Gamma = 10$. Panel (a) shows results for a system without friction while in panel (b) the friction coefficient is $\nu/\omega_p = 0.2$. Numbers in the figure denote the wavenumber, ka.

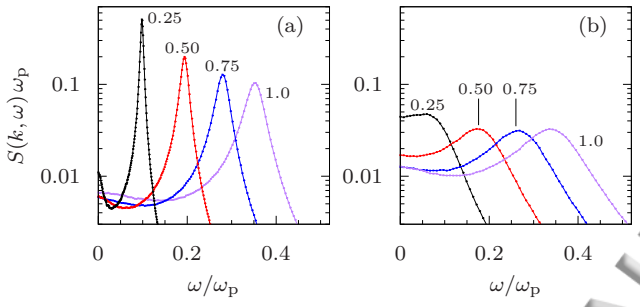

FIG. 5. Dynamic structure factor for a system with screening parameter $\kappa = 2$ and coupling parameter $\Gamma = 200$. Panel (a) shows results for a system without friction while in panel (b) the friction coefficient is $\nu/\omega_p = 0.1$. Numbers in the figure denote the wavenumber, ka.

the wavenumber is decreased. Here, the well-known hydrodynamic behavior with a two-peak structure can be observed, representing the Brillouin and Rayleigh peak. In contrast, the behavior for the system with dissipation is vastly different. The height of the sound peak shows a slight increase towards smaller ka but, at the same time, the DSF increases faster at $\omega = 0$. In particular, the finite-frequency sound peak completely disappears for small ka, see Fig. 4(b). At the smallest wavenumber, $ka = 0.25$, only a single maximum at zero frequency remains. For the system with $\Gamma = 200$, a very weak maximum at finite ω persists at $ka = 0.25$. As discussed in Ref. 58, the sound mode can be considered overdamped in this limit. In Fig. 6, the position of the sound peak in the DSF is shown for different values of the friction coefficient.[59] Damping generally leads to a red-shift of the frequency, as discussed in Sec. III.1. Below a certain cutoff wavenumber, which is rather sensitive to the value of ν/ω_p, the sound peak at finite ω vanishes, as demonstrated in Fig. 4. Note that, for $\nu/\omega_p = 0.1$, a very weak peak persists at the smallest wavenumber available in the simulation.

The damping of the sound mode, as measured by the FWHM (full-width at half maximum), denoted $\Delta\omega$, is shown in Fig. 7(a) for the system with $\Gamma = 10$ at two different wavenumbers. The peak width increases with the friction coefficient in a way that slightly exceeds a linear behavior, $\Delta\omega(\nu) = \Delta\omega_0 + \nu$, as indicated by the dashed lines. At the same time, the peak height drops rapidly with ν, see Fig. 7(b).

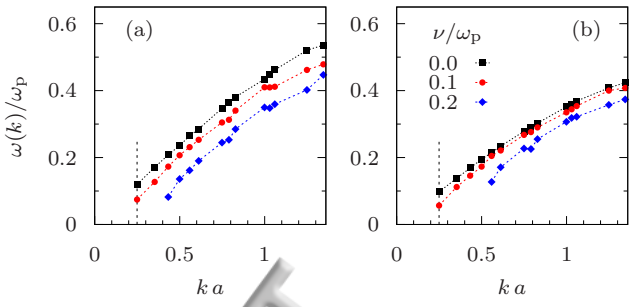

FIG. 6. Peak position as obtained from the DSF as a function of the wavenumber for various values of the friction coefficient, as indicated in the figure. The coupling parameter is (a) $\Gamma = 10$ and (b) $\Gamma = 200$. The vertical dashed lines indicate the lowest available wavenumber.

As an example, a friction coefficient $\nu/\omega_p = 0.01$, amounting to less than 10% of the frequency of the sound mode at the wavenumber $ka = 0.25$, is sufficient to decrease the peak height by a factor two. This demonstrates again the high sensitivity of the sound mode to even a small amount of friction,[10] in particular at small wavenumbers. For a related investigation of the longitudinal current spectrum in a 2D Yukawa plasma, see Ref. 12, where similar observations concerning the height and width of the sound peak have been reported.

The behavior described above is reminiscent of a damped harmonic oscillator. If the damping rate ν is much smaller than the natural oscillator frequency, ω_0, the oscillations are weakly damped (underdamped), with an effective oscillation frequency that is below ω_0 and that decreases with the damping. For damping rates much larger than ω_0, on the other hand, the oscillatory behavior disappears (overdamped limit). Provided the ISF at small k can be approximately described as a damped oscillator with a wavenumber dependent frequency, $\omega_0(k)$, this could explain (i) the red-shift of the peak position, (ii) the increase of the peak width with increasing ν (damping), and (iii) the observation that the sound peak at small k vanishes prior to the sound mode at larger k. The reason for (iii) is that the frequency increases with the wavenumber, approximately $\omega_0(k) \propto k$. Thus, the overdamped limit is reached earlier at small k. Note, however, that other effects such as viscous damping or the thermal mode have been disregarded. In the context of the memory function formalism, a damped harmonic oscillator model has been discussed as a simplified hydrodynamic description for the ISF and the DSF of frictionless systems, where the ratio of specific heats is exactly $\gamma = 1$.[60] For a memory function description with frictional damping, see Refs. 13 and 58.

In the following, the low-frequency part of the DSF around $\omega = 0$ will be inspected more closely. It has already been noted in Sec. III.1 that the DSF displays a non-monotonic dependence on the friction coefficient in this domain. This is illustrated in Figure 8 in more detail, where the DSF is shown for low damping, $\nu/\omega_p \leq 0.1$. As the inset shows, the peak height at $\omega = 0$ initially decreases and reaches a minimum around $\nu/\omega_p \approx 0.02$. From this point, the zero frequency peak increases while, at the same time, the sound mode becomes significantly weaker, and only a weak remnant remains

ACCEPTED MANUSCRIPT

This manuscript was accepted by Phys. Plasmas. Click here to see the version of record.

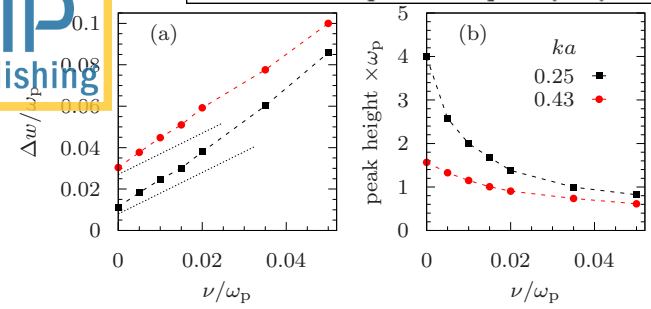

FIG. 7. (a) FWHM $\Delta\omega(\nu)$ and (b) peak height of the sound mode at two different wavenumbers, as indicated in the figure. The dotted lines in panel (a) depict a linear behavior, $\Delta\omega(\nu) = \Delta\omega_0 + \nu$. The screening parameter is $\kappa = 2$, the coupling is $\Gamma = 10$.

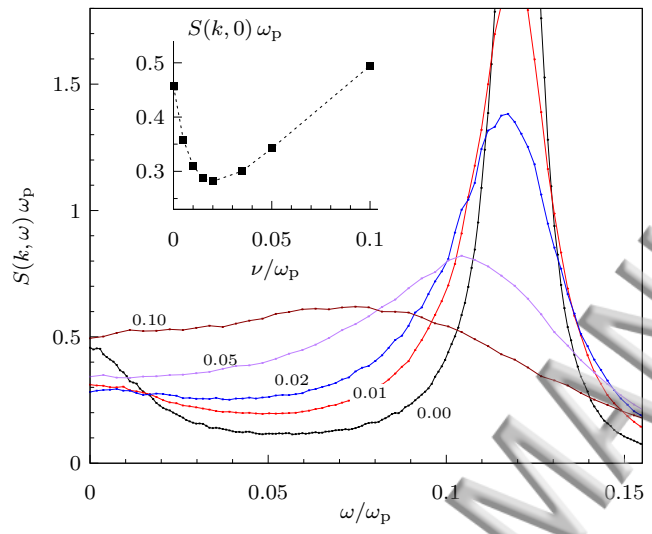

FIG. 8. Dynamic structure factor in the low-frequency domain at $ka = 0.25$ for a system with $\kappa = 2$ and $\Gamma = 10$. Numbers in the figure denote the value of ν/ω_p. The inset shows the peak height at zero frequency as a function of the damping.

at $\nu/\omega_p \approx 0.1$, see also Fig. 2(a)

III.3. Large wavenumbers

At high wavenumbers, i.e., on small length scales, the DSF can be compared with the result for non-interacting particles. For strongly coupled Yukawa plasmas without friction, the transition to free particle (ideal gas) behavior has been investigated in Ref. 57. In this section, the effect of friction on the DSF at large wavenumbers is studied by comparing the simulation results with analytical limits for a damped system of non-interacting particles, which are briefly reviewed first.

The ISF for a single Brownian particle described by the Langevin equation, Eq. (3), can be written as $F_s(\boldsymbol{k},t) = \exp\left[-\frac{k^2}{6}\langle \boldsymbol{r}^2(t)\rangle\right]$,[58] where the mean-squared-displacement is given by

$$\langle \boldsymbol{r}^2(t)\rangle = 6\,(v_{th}^2/\nu^2)\,\{\nu t + [\exp(-\nu t) - 1]\}\,. \qquad (6)$$

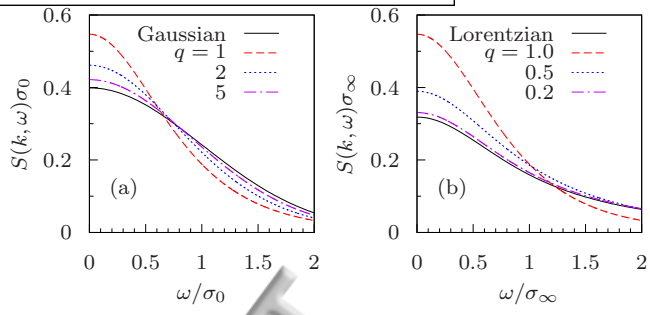

FIG. 9. Dynamic structure factor of the single-particle (non-interacting) system, calculated using Eq. (7), for various values of q. The DSF for the ideal gas (Gaussian) and the Lorentzian approximation are shown for comparison in panels (a) and (b), respectively. Note the different scaling of the axes.

The thermal velocity is $v_{th} = \sqrt{k_B T/m}$. For comparison with the simulations, the ISF must be converted into frequency space. The Laplace transform of the ISF can be written in terms of the confluent hypergeometric function, ${}_1F_1(a,c;z)$, as

$$\tilde{F}_s(\boldsymbol{k},\omega) = \frac{1}{\nu}\frac{{}_1F_1(1, q^2 - i\omega/\nu + 1; q^2)}{q^2 - i\omega/\nu}, \qquad (7)$$

where $q = k v_{th}/\nu$ is a dimensionless wavenumber, see Appendix A. The DSF is then calculated from $S_s(\boldsymbol{k},\omega) = \mathrm{Re}\,\tilde{F}_s(\boldsymbol{k},\omega)/\pi$.

There exist two important limiting cases. In the free-particle (Newtonian, $\nu = 0$) limit, the single-particle DSF has a Gaussian shape, $S_s(\boldsymbol{k},\omega) = (2\pi\sigma_0^2)^{-1/2}\exp(-\omega^2/2\sigma_0^2)$, where $\sigma_0 = k v_{th}$.[49,51,57] This can be obtained by using the short-time (ballistic) limit of Eq. (6), $\langle \boldsymbol{r}^2(t)\rangle \approx 3 v_{th}^2 t^2$, for the calculation of the Laplace transform. On the other hand, in the long-time limit, $\nu t \gg 1$, the mean-squared displacement shows diffusive behavior, $\langle \boldsymbol{r}^2(t)\rangle \approx 6 D_0 t$, with $D_0 = k_B T/(m\nu)$ being the diffusion coefficient of the ideal system. When the ISF decays strictly exponentially, a Lorentzian shape is obtained, $S_s(\boldsymbol{k},\omega) = (\sigma_\infty/\pi)/\left(\omega^2 + \sigma_\infty^2\right)$, where $\sigma_\infty = k^2 v_{th}^2/\nu$.[49] Figure 9 shows the single-particle DSF for various values of q. For large q, i.e., on length scales much smaller than v_{th}/ν [Fig. 9(a)], the DSF almost acquires a Gaussian shape while for small q [Fig. 9(b)], the DSF resembles the Lorentzian. Note, however, that the high-frequency limits are different.

The analytical results can now be compared with the large wavenumber DSF of the interacting system. Figure 10 shows results for the system with $\Gamma = 10$. Note that the values for $S(k)$ are close to unity for these parameters, see Fig. 1(a). For $ka = 5.25$ [Fig. 10(a)], there are still substantial deviations between the non-interacting DSF and the simulations while they are significantly reduced at $ka = 7.38$ [Fig. 10(b)]. Here, for $\nu = 0$, the simulations are in excellent agreement with the ideal gas DSF, which indicates that interaction effects are weak. On the other hand, frictional damping strongly affects the DSF and increases (decreases) the DSF at low (high) frequencies. The deviations are well captured by Eq. (7), which accounts for friction but still neglects interactions. The reduced wavenumber q takes on values $q \approx 2.7$ for $\nu/\omega_p = 0.5$

ACCEPTED MANUSCRIPT

AIP Publishing

This manuscript was accepted by Phys. Plasmas. Click here to see the version of record.

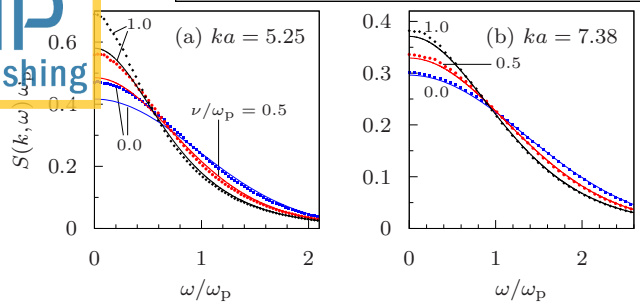

FIG. 10. Dynamic structure factor for a system with $\Gamma = 10$ and $\kappa = 2$ at two wavenumbers. Numbers in the figure denote the value of ν/ω_p. The symbols correspond to the simulation results, and the lines show the analytical result for the single-particle DSF.

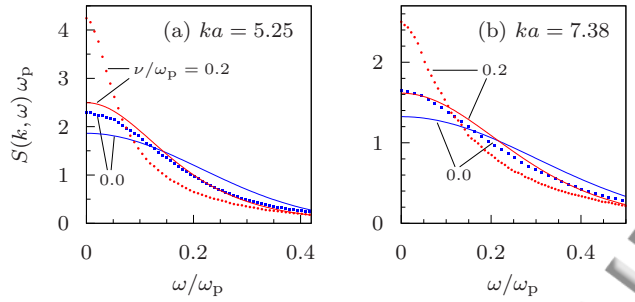

FIG. 11. Dynamic structure factor for a system with $\Gamma = 200$ and $\kappa = 2$ at two wavenumbers. Numbers in the figure denote the value of ν/ω_p. The symbols correspond to the simulation results, and the lines show the analytical result for the single-particle DSF.

and $q \approx 1.3$ for $\nu/\omega_p = 1$ at $ka = 7.38$. Figure 9(a) shows that deviations from the Gaussian shape are to be expected at these parameters if the single-particle description is applicable.

Figure 11 shows the same comparison for $\Gamma = 200$. The deviations between the single-particle DSF and the simulation results are significantly larger than for $\Gamma = 10$. Similar observations have been made in Ref. 57 for Yukawa plasmas without dissipation, where the ideal gas limit provided a better description for the DSF in the case of more weakly coupled systems. Similar to the results shown in Fig. 10, friction leads to a more narrow peak. Note that even though $S(k) \approx 1$ for the specific wavenumbers shown in Fig. 11, the static structure factor still shows substantial oscillations around one in this wavenumber region, see Fig. 1(a).

IV. CONCLUSION

In summary, the DSF of the strongly coupled Yukawa plasma has been studied with molecular and Langevin dynamics simulations over a wide range of friction coefficients and wavenumbers. The simulations show that frictional damping can have a large effect on the DSF. In general, it decreases the height of the sound peak and leads to a red-shift of its frequency. In the high damping limit, the DSF develops a strong maximum at zero frequency. For intermediate wavenumbers and very strong coupling, a narrow zero frequency peak is followed by a much slower decay of the DSF towards higher frequencies.

Friction has a particularly strong effect on the small wavenumber limit. The simulations show that a sound peak at finite ω, which exists for intermediate wavenumbers, may disappear at smaller k and transform into a peak at zero frequency. This is in stark contrast to frictionless simulations, where two well-defined Rayleigh- and Brillouin modes at $\omega = 0$ and at finite ω, respectively, are observed at small wavenumbers. A theoretical treatment of this aspect can be found in Ref. 58. Simulations with different ν at a small wavenumber, where a well-defined Rayleigh peak exists for $\nu = 0$, show that weak damping can initially reduce its height. In this case, the DSF shows a non-monotonic behavior as a function of the friction coefficient at $\omega = 0$. It would be interesting to study this effect in systems that exhibit a stronger Rayleigh peak, which is usually weak in strongly coupled Yukawa plasmas.

In order to decipher the individual contributions of the thermal mode and the sound mode to the DSF, one could compare the simulation results with a memory function description,[49–51,60] where frictional damping is included.[13,58] It has already been shown that the DSF of the strongly coupled Yukawa OCP without friction is well described in terms of a single Gaussian term in the memory function.[57] However, this model does not account for the thermal mode, whose contribution could be added to the memory function. While its contribution to the DSF is small, it contains important information on the thermodynamic and transport properties of the plasma, e.g., the thermal diffusivity.[51] Further, this might allow one to develop a better understanding of the influence of friction on the thermal (Rayleigh) mode.

ACKNOWLEDGMENTS

Fruitful discussions with Zh. Moldabekov and M. Bonitz are gratefully acknowledged.

Appendix A: Laplace transform of the single particle ISF

Using Eq. (6) and $F_s(\boldsymbol{k},t) = \exp\left[-\frac{k^2}{6}\langle \boldsymbol{r}^2(t)\rangle\right]$[58] one obtains

$$\begin{aligned}\tilde{F}_s(\boldsymbol{k},\omega) &= \int_0^\infty e^{i\omega t} F_s(\boldsymbol{k},t)\,\mathrm{d}t \\ &= \int_0^\infty e^{-\nu t(q^2 - i\omega/\nu) - q^2\left(e^{-\nu t}-1\right)}\,\mathrm{d}t \\ &= \nu^{-1} e^{q^2}\,(q^2)^{-q^2 + i\omega/\nu}\,\gamma(q^2 - i\omega/\nu, q^2), \qquad \text{(A1)}\end{aligned}$$

where $\gamma(a,z) = \int_0^z y^{a-1}e^{-y}\,dy$ is the incomplete Gamma function.[61] The result can also be expressed in terms of Kummer's confluent hypergeometric function, ${}_1F_1(a,c;z)$, which is related to the incomplete Gamma function via $\gamma(a,z) = a^{-1}z^a e^{-z}\,{}_1F_1(1,a+1;z)$.[61] This relation leads to Eq. (7) in the main text. One identifies the denominator of Eq. (7) with the Laplace transform of the overdamped (diffusive) limit for the ISF.

ACCEPTED MANUSCRIPT

This manuscript was accepted by Phys. Plasmas. Click here to see the version of record.

[1] S. H. Glenzer, L. B. Fletcher, E. Galtier, B. Nagler, R. Alonso-Mori, B. Barbrel, S. B. Brown, D. A. Chapman, Z. Chen, C. B. Curry, F. Fiuza, E. Gamboa, M. Gauthier, D. O. Gericke, A. Gleason, S. Goede, E. Granados, P. Heimann, J. Kim, D. Kraus, M. J. MacDonald, A. J. Mackinnon, R. Mishra, A. Ravasio, C. Roedel, P. Sperling, W. Schumaker, Y. Y. Tsui, J. Vorberger, U. Zastrau, A. Fry, W. E. White, J. B. Hasting, and H. J. Lee, J. Phys. B: At. Mol. Opt. Phys. **49**, 092001 (2016).

[2] F. Graziani, M. P. Desjarlais, R. Redmer, and S. B. Trickey, eds., *Frontiers and Challenges in Warm Dense Matter* (Springer International Publishing, Cham, 2014).

[3] M. Lyon and S. L. Rolston, Rep. Prog. Phys. **80**, 017001 (2017).

[4] M. Bonitz, C. Henning, and D. Block, Rep. Prog. Phys. **73**, 066501 (2010).

[5] O. A. Hurricane, D. A. Callahan, D. T. Casey, P. M. Celliers, C. Cerjan, E. L. Dewald, T. R. Dittrich, T. Döppner, D. E. Hinkel, L. F. Berzak Hopkins, J. L. Kline, S. LePape, T. Ma, A. G. MacPhee, J. L. Milovich, A. Pak, H.-S. Park, P. K. Patel, B. A. Remington, J. D. Salmonson, P. T. Springer, and R. Tommasini, Nature **506**, 343 (2014).

[6] R. S. Craxton, K. S. Anderson, T. R. Boehly, V. N. Goncharov, D. R. Harding, J. P. Knauer, R. L. McCrory, P. W. McKenty, D. D. Meyerhofer, J. F. Myatt, A. J. Schmitt, J. D. Sethian, R. W. Short, S. Skupsky, W. Theobald, W. L. Kruer, K. Tanaka, R. Betti, T. J. B. Collins, J. A. Delettrez, S. X. Hu, J. A. Marozas, A. V. Maximov, D. T. Michel, P. B. Radha, S. P. Regan, T. C. Sangster, W. Seka, A. A. Solodov, J. M. Soures, C. Stoeckl, and J. D. Zuegel, Phys. Plasmas **22**, 110501 (2015).

[7] J. J. Fortney and N. Nettelmann, Space Sci. Rev. **152**, 423 (2010).

[8] T. S. Strickler, T. K. Langin, P. McQuillen, J. Daligault, and T. C. Killian, Phys. Rev. X **6**, 021021 (2016).

[9] G. E. Morfill, A. V. Ivlev, and H. M. Thomas, Phys. Plasmas **19**, 055402 (2012).

[10] P. Mabey, S. Richardson, T. White, L. Fletcher, S. Glenzer, N. Hartley, J. Vorberger, D. Gericke, and G. Gregori, Nat. Commun. **8**, 14125 (2017).

[11] J. Dai, Y. Hou, and J. Yuan, Phys. Rev. Lett. **104**, 245001 (2010).

[12] L.-J. Hou, Z. L. Mišković, A. Piel, and M. S. Murillo, Phys. Rev. E **79**, 046412 (2009).

[13] N. Upadhyaya, Z. L. Mikovi, and L.-J. Hou, New J. Phys. **12**, 093034 (2010).

[14] N. Upadhyaya, V. Nosenko, Z. L. Mikovi, L.-J. Hou, A. V. Ivlev, and G. E. Morfill, EPL **94**, 65001 (2011).

[15] T. Ott, M. Bonitz, P. Hartmann, and Z. Donkó, Phys. Rev. E **83**, 046403 (2011).

[16] W. Kong, S. Liu, F. Yang, F. Shi, and Y. Wang, Phys. Plasmas **25**, 083709 (2018).

[17] M. Rosenberg and G. Kalman, Phys. Rev. E **56**, 7166 (1997).

[18] X. Wang, A. Bhattacharjee, and S. Hu, Phys. Rev. Lett. **86**, 2569 (2001).

[19] H. Löwen, J.-P. Hansen, and J.-N. Roux, Phys. Rev. A **44**, 1169 (1991).

[20] H. Löwen, Phys. Rep. **237**, 249 (1994).

[21] H. Acuña Campa and M. Medina-Noyola, J. Chem. Phys. **113**, 869 (2000).

[22] P. Hartmann, Z. Donkó, T. Ott, H. Kählert, and M. Bonitz, Phys. Rev. Lett. **111**, 155002 (2013).

[23] A. Melzer, M. Himpel, H. Krüger, M. Mulsow, and S. Schütt, Plasma Phys. Control. Fusion **61**, 014029 (2018).

[24] T. G. White, S. Richardson, B. J. B. Crowley, L. K. Pattison, J. W. O. Harris, and G. Gregori, Phys. Rev. Lett. **111**, 175002 (2013).

[25] H. R. Rüter and R. Redmer, Phys. Rev. Lett. **112**, 145007 (2014).

[26] B. B. L. Witte, M. Shihab, S. H. Glenzer, and R. Redmer, Phys. Rev. B **95**, 144105 (2017).

[27] J. Vorberger, Z. Donkó, I. M. Tkachenko, and D. O. Gericke, Phys. Rev. Lett. **109**, 225001 (2012).

[28] L. Harbour, G. D. Förster, M. W. C. Dharma-wardana, and L. J. Lewis, Phys. Rev. E **97**, 043210 (2018).

[29] Z. A. Moldabekov, H. Kählert, T. Dornheim, S. Groth, M. Bonitz, and T. S. Ramazanov, Phys. Rev. E **99**, 053203 (2019).

[30] E. E. McBride, T. G. White, A. Descamps, L. B. Fletcher, K. Appel, F. P. Condamine, C. B. Curry, F. Dallari, S. Funk, E. Galtier, M. Gauthier, S. Goede, J. B. Kim, H. J. Lee, B. K. Ofori-Okai, M. Oliver, A. Rigby, C. Schoenwaelder, P. Sun, T. Tschentscher, B. B. L. Witte, U. Zastrau, G. Gregori, B. Nagler, J. Hastings, S. H. Glenzer, and G. Monaco, Rev. Sci. Instrum. **89**, 10F104 (2018).

[31] P. Ludwig, W. J. Miloch, H. Kählert, and M. Bonitz, New J. Phys. **14**, 053016 (2012).

[32] P. Ludwig, H. Kählert, and M. Bonitz, Plasma Phys. Control. Fusion **54**, 045011 (2012).

[33] J.-P. Joost, P. Ludwig, H. Kählert, C. Arran, and M. Bonitz, Plasma Phys. Control. Fusion **57**, 025004 (2015).

[34] K. Wünsch, J. Vorberger, and D. O. Gericke, Phys. Rev. E **79**, 010201 (2009).

[35] A. Schella, M. Mulsow, A. Melzer, H. Khlert, D. Block, P. Ludwig, and M. Bonitz, New J. Phys. **15**, 113021 (2013).

[36] Z. Donkó, G. J. Kalman, and P. Hartmann, J. Phys.: Condens. Matter **20**, 413101 (2008).

[37] M. Bonitz, Z. Donkó, T. Ott, H. Kählert, and P. Hartmann, Phys. Rev. Lett. **105**, 055002 (2010).

[38] T. Ott, H. Löwen, and M. Bonitz, Phys. Rev. Lett. **111**, 065001 (2013).

[39] Y. Feng, J. Goree, B. Liu, T. P. Intrator, and M. S. Murillo, Phys. Rev. E **90**, 013105 (2014).

[40] H. Ohta and S. Hamaguchi, Phys. Rev. Lett. **84**, 6026 (2000).

[41] J. P. Mithen, J. Daligault, and G. Gregori, Phys. Rev. E **83**, 015401(R) (2011).

[42] T. Ott, M. Bonitz, L. G. Stanton, and M. S. Murillo, Phys. Plasmas **21**, 113704 (2014).

[43] J. P. Mithen, Phys. Rev. E **89**, 013101 (2014).

[44] T. Ott, M. Bonitz, and Z. Donkó, Phys. Rev. E **92**, 063105 (2015).

[45] S. A. Khrapak, I. L. Semenov, L. Couëdel, and H. M. Thomas, Phys. Plasmas **22**, 083706 (2015).

[46] T. Ott, M. Bonitz, P. Hartmann, and Z. Donkó, Phys. Rev. E **95**, 013209 (2017).

[47] H. Kählert and M. Bonitz, Phys. Rev. E **83**, 056401 (2011).

[48] R. Mannella, Phys. Rev. E **69**, 041107 (2004).

[49] J. P. Boon and S. Yip, *Molecular hydrodynamics* (New York, Dover publications, 1991).

[50] U. Balucani and M. Zoppi, *Dynamics of the Liquid State* (Clarendon Press, Oxford, 1995).

[51] J. P. Hansen and I. R. McDonald, *Theory of Simple Liquids* (Elsevier Academic Press, London, 2006).

[52] The code has been implemented in the *Julia* language[53].

[53] J. Bezanson, A. Edelman, S. Karpinski, and V. Shah, SIAM Rev. **59**, 65 (2017).

[54] T. Ott, H. Kählert, A. Reynolds, and M. Bonitz, Phys. Rev. Lett. **108**, 255002 (2012).

[55] I. Korolov, G. J. Kalman, L. Silvestri, and Z. Donkó, Contrib. Plasma Phys. **55**, 421 (2015).

[56] W. H. Press, S. A. Teukolsky, W. T. Vetterling, and B. P. Flannery, *Numerical Recipes: The Art of Scientific Computing*, 3rd ed. (Cambridge University Press, Cambridge, 2007).

[57] J. P. Mithen, J. Daligault, B. J. B. Crowley, and G. Gregori, Phys. Rev. E **84**, 046401 (2011).

[58] W. Hess and R. Klein, Adv. Phys. **32**, 173 (1983).

[59] Note that the data for finite ν have a larger scatter, partly because the maximum becomes very weak for small wavenumbers.

[60] U. Bafile, E. Guarini, and F. Barocchi, Phys. Rev. E **73**, 061203 (2006).

[61] G. B. Arfken and H. J. Weber, *Mathematical Methods for Physicists*, 6th ed. (Elsevier Academic Press, New York, 2005).

ACCEPTED MANUSCRIPT

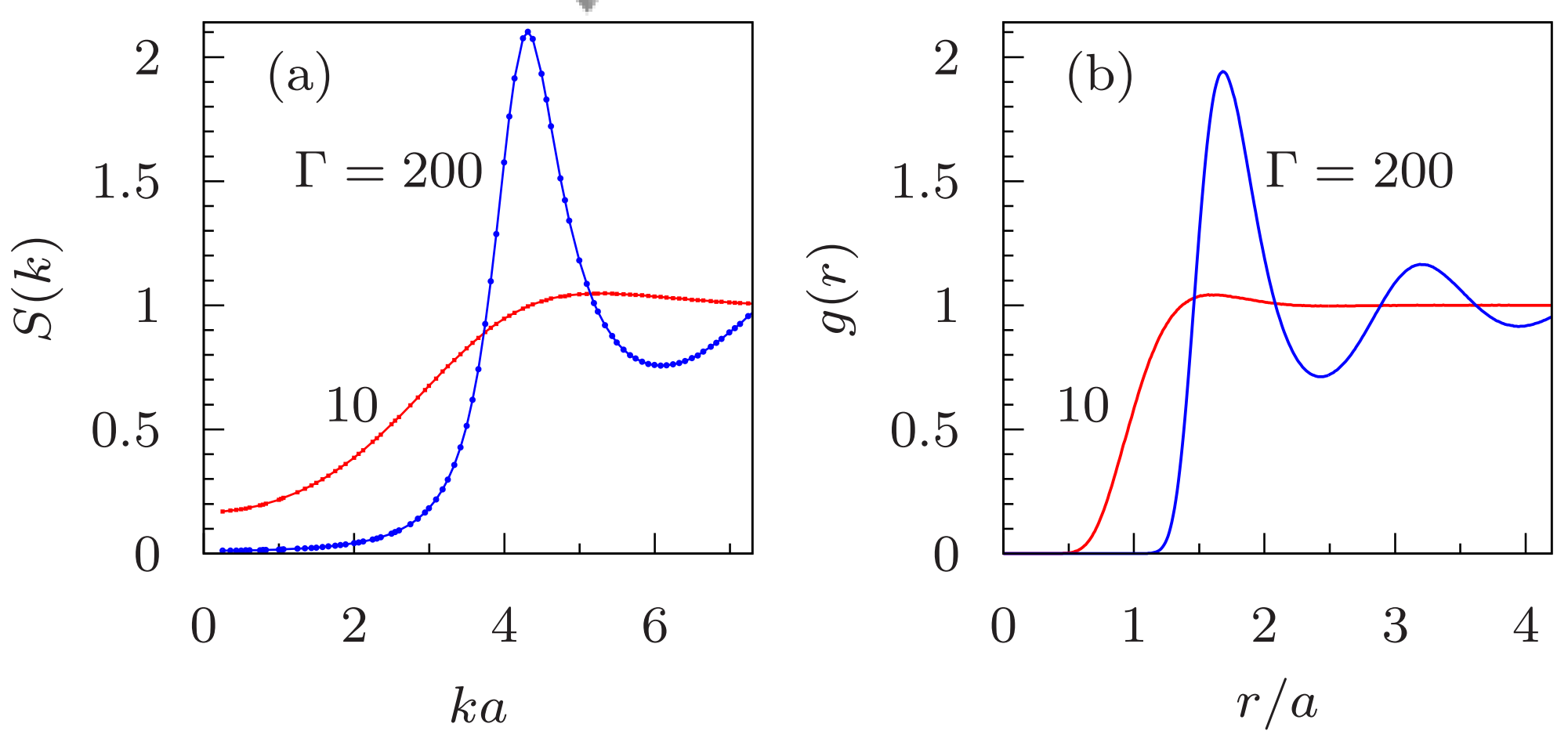
(a)
$\Gamma = 200$
10
$S(k)$
ka
0
0.5
1
1.5
2
0
2
4
6
(b)
$\Gamma = 200$
10
$g(r)$
r/a
0
0.5
1
1.5
2
0
1
2
3
4

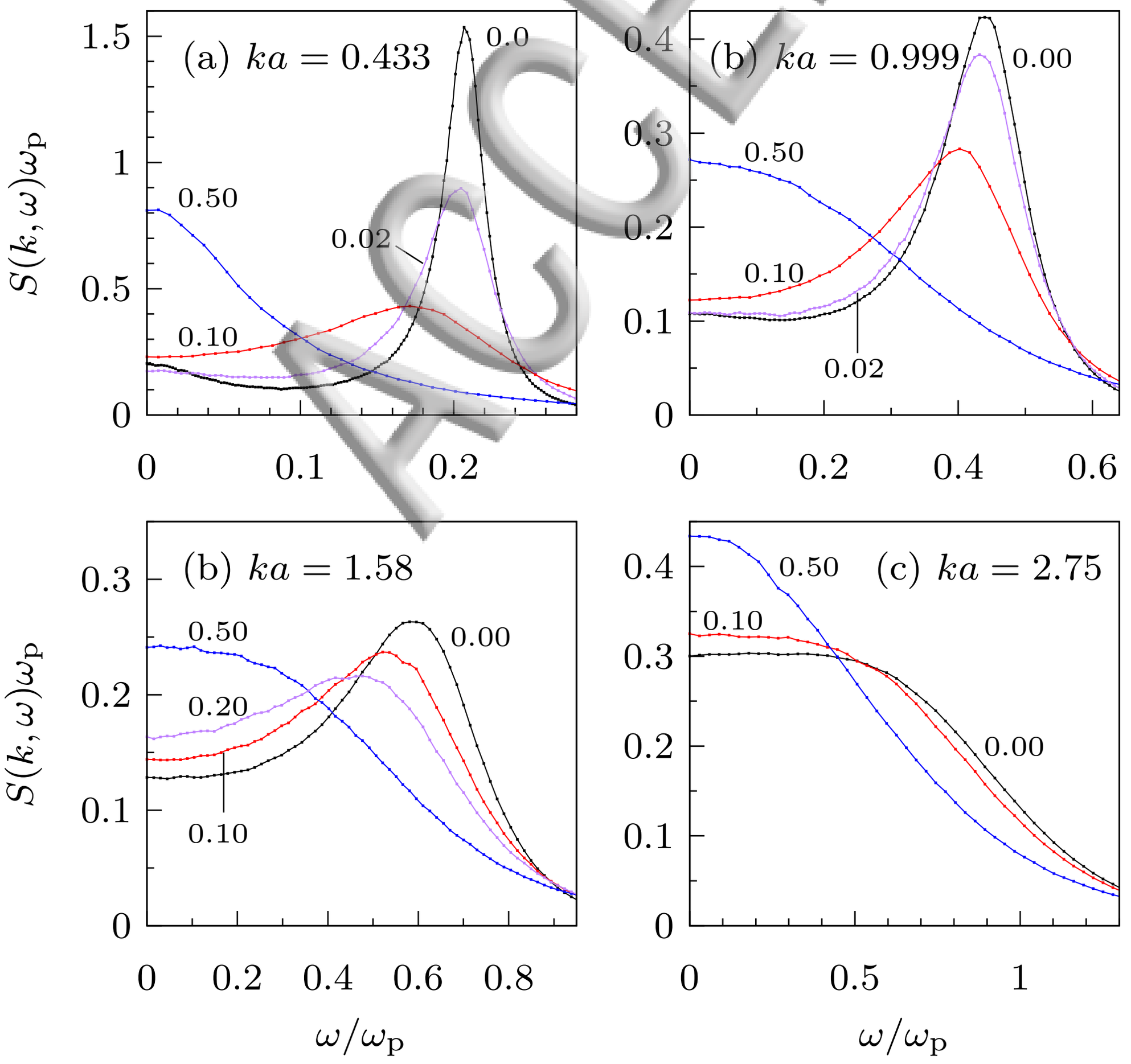
(a) $ka = 0.433$
0.0
0.50
0.02
0.10
(b) $ka = 0.999$
0.00
0.50
0.10
0.02
(b) $ka = 1.58$
0.50
0.00
0.20
0.10
(c) $ka = 2.75$
0.50
0.10
0.00
$S(k,\omega)\omega_p$
ω/ω_p

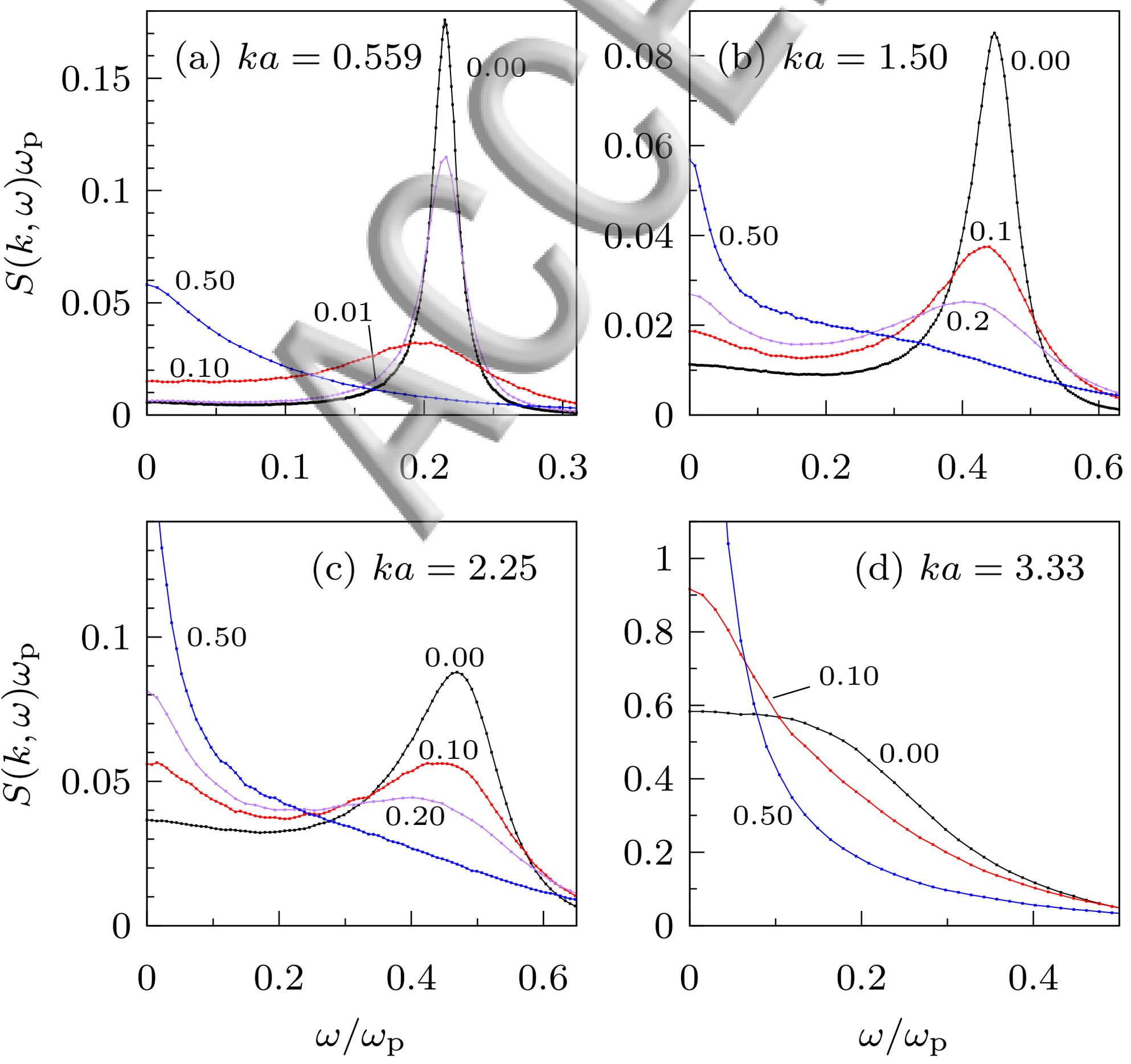
(a) $ka = 0.559$
(b) $ka = 1.50$
(c) $ka = 2.25$
(d) $ka = 3.33$
$S(k,\omega)\omega_p$
ω/ω_p
0.00
0.01
0.10
0.20
0.50
0.1
0.2
0.4
0.6
0.8
1

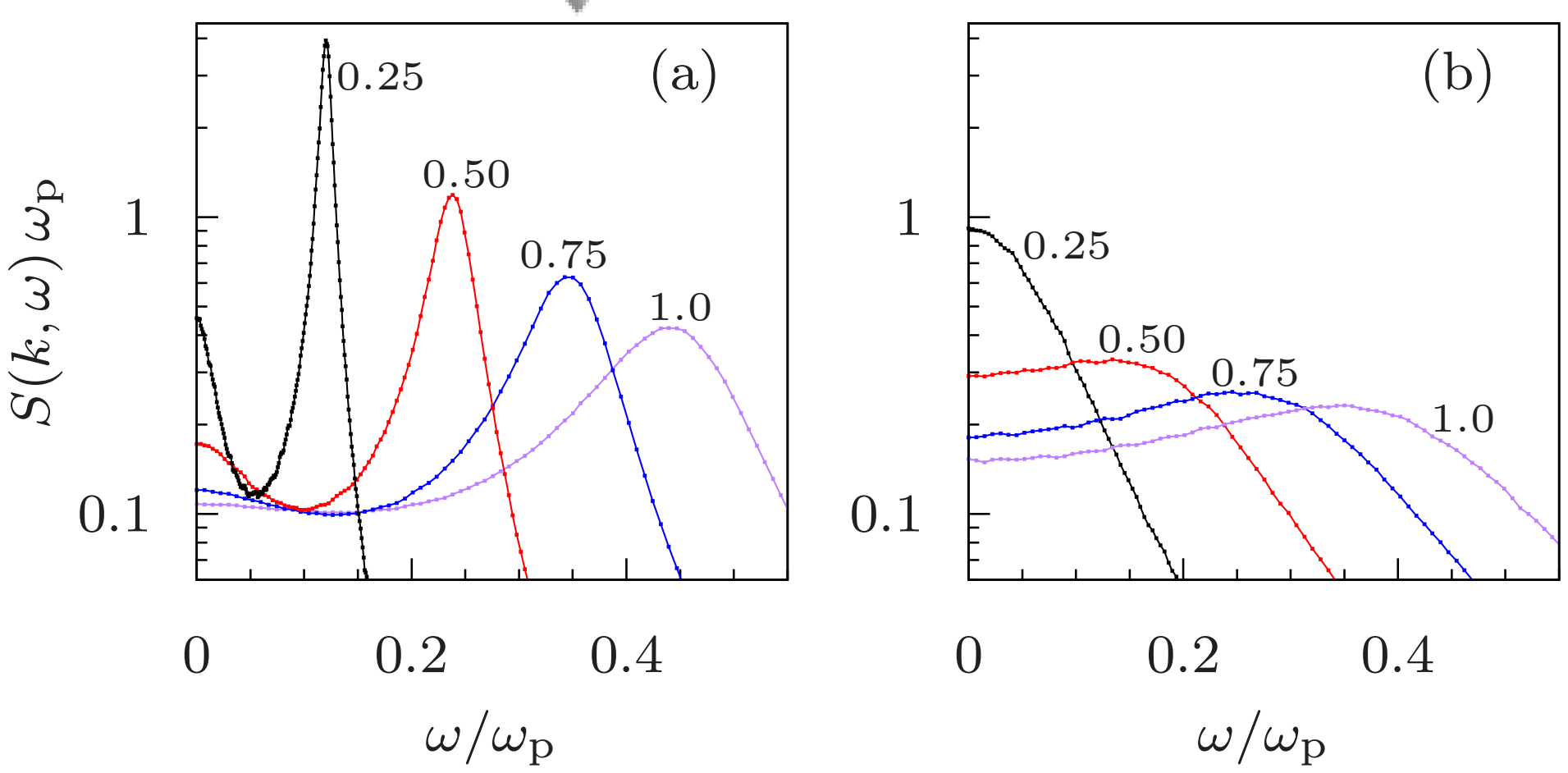
(a)
(b)
0.25
0.50
0.75
1.0
1
0.1
$S(k,\omega)\,\omega_{\rm p}$
0
0.2
0.4
$\omega/\omega_{\rm p}$

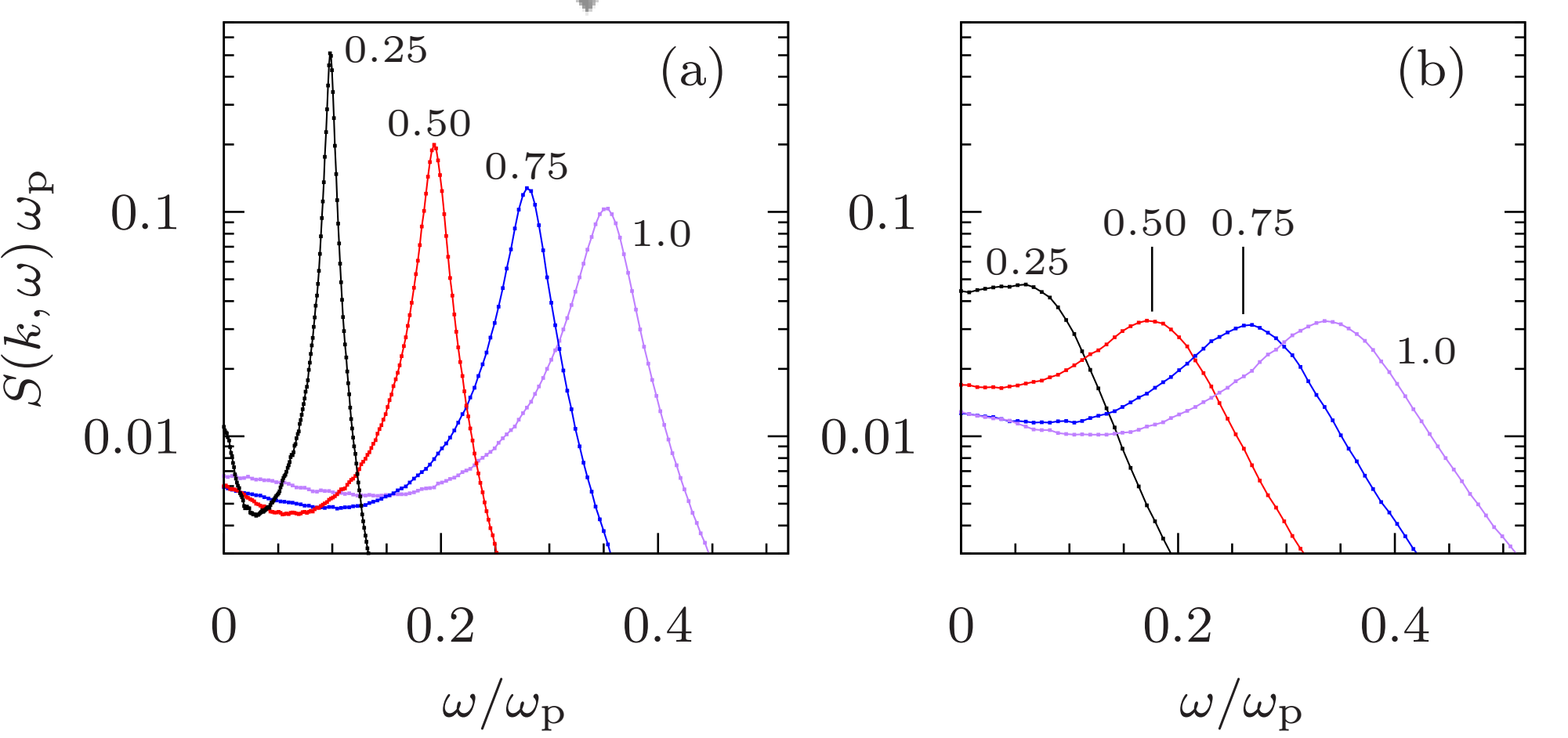
$S(k,\omega)\,\omega_p$
0.1
0.01
0.25
0.50
0.75
1.0
(a)
0
0.2
0.4
ω/ω_p
0.1
0.01
0.25
0.50
0.75
1.0
(b)
0
0.2
0.4
ω/ω_p

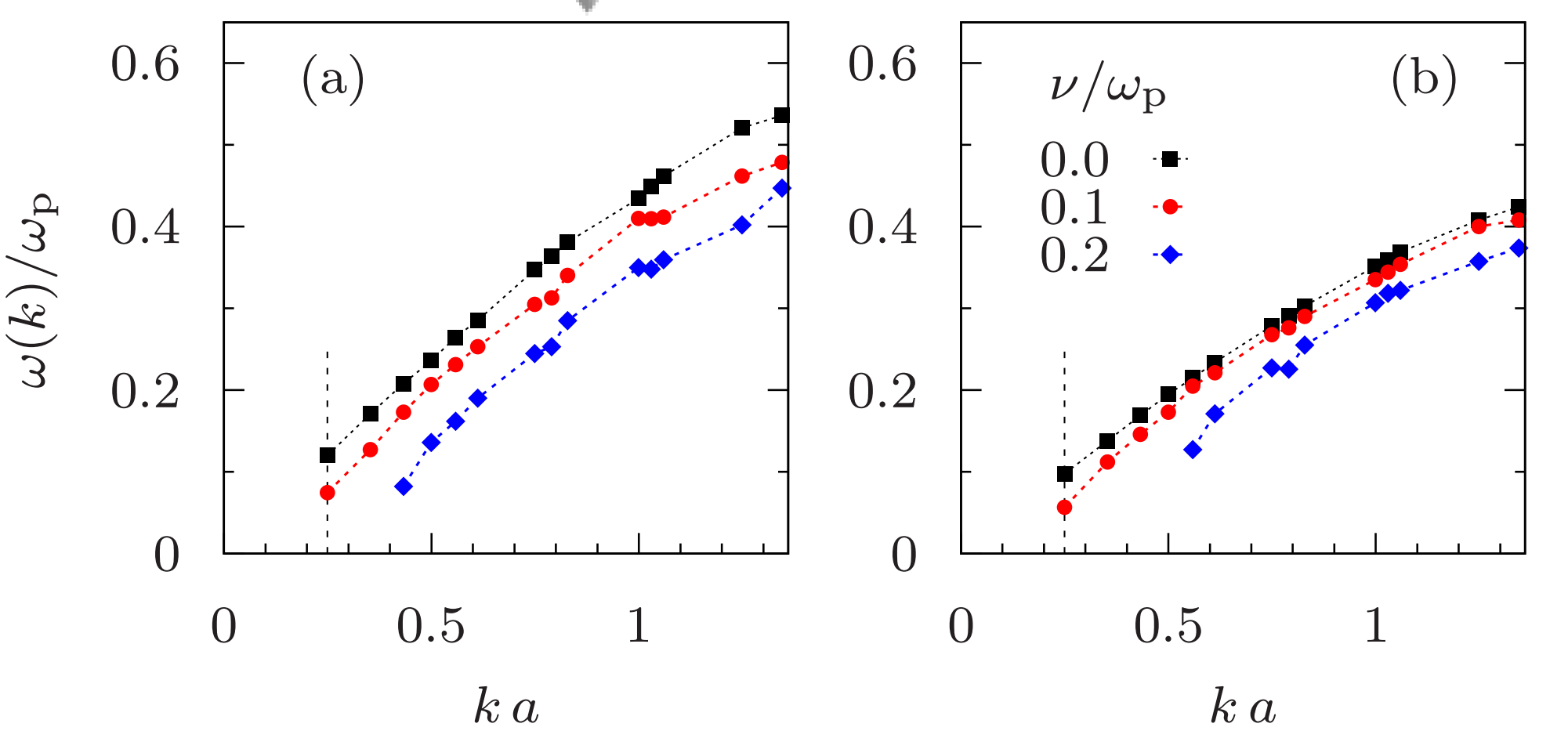
(a)
(b)
$\omega(k)/\omega_p$
$k\,a$
ν/ω_p
0.0
0.1
0.2
0
0.2
0.4
0.6
0.5
1

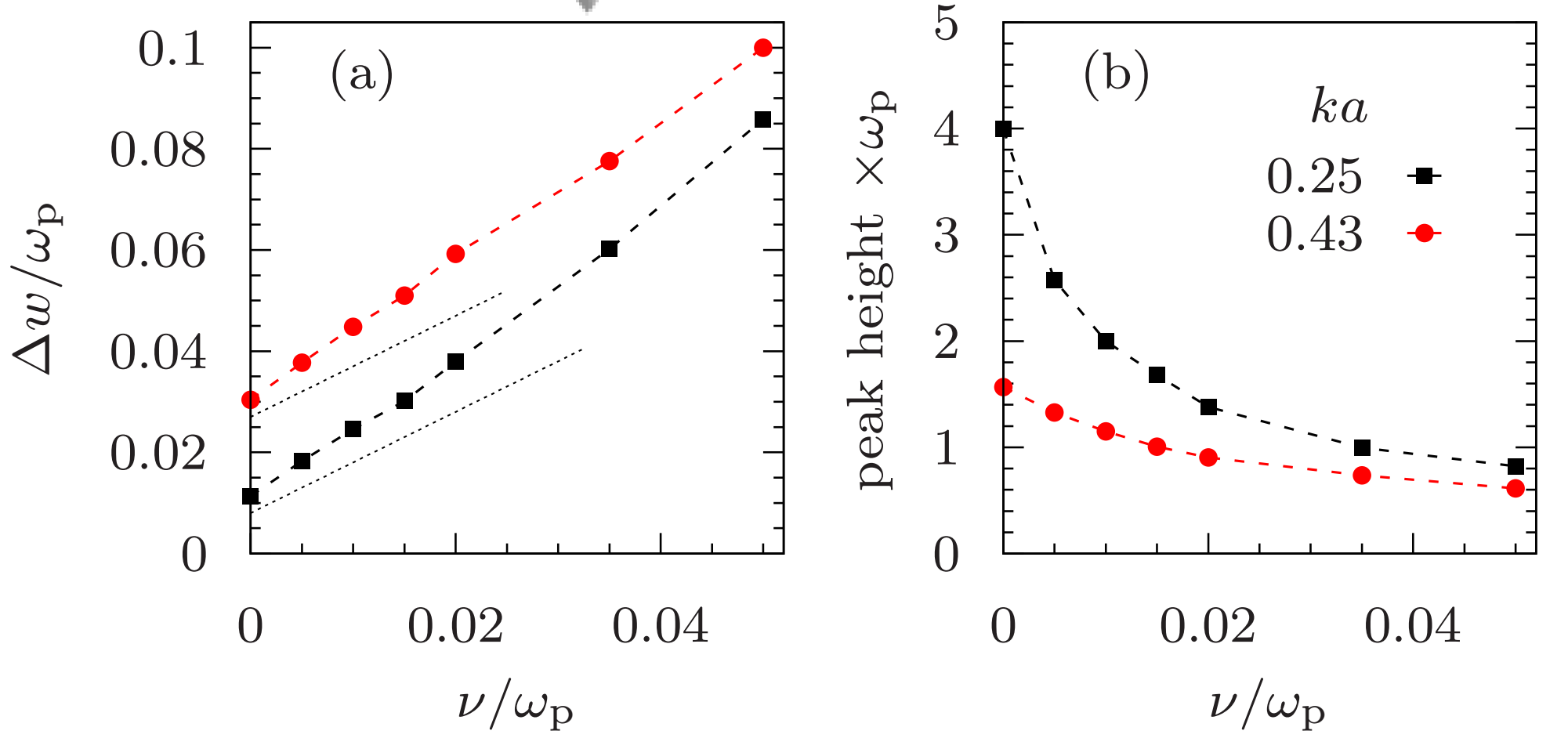
(a)
0.1
0.08
0.06
0.04
0.02
0
$\Delta w/\omega_p$
0
0.02
0.04
ν/ω_p
(b)
ka
0.25
0.43
peak height $\times\omega_p$
5
4
3
2
1
0
0
0.02
0.04
ν/ω_p

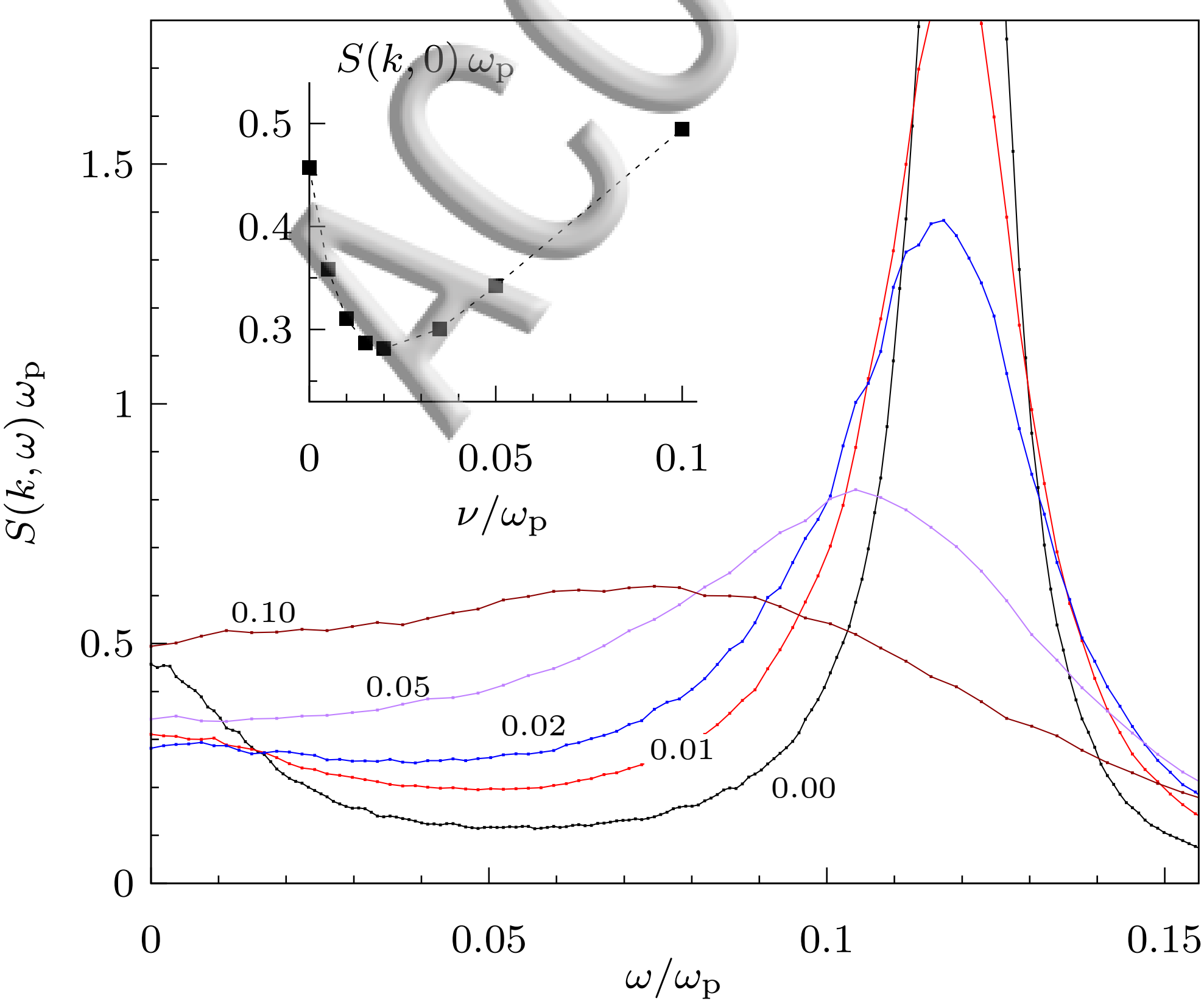
$S(k,0)\,\omega_\mathrm{p}$
0.5
0.4
0.3
0
0.05
0.1
ν/ω_p
$S(k,\omega)\,\omega_\mathrm{p}$
1.5
1
0.5
0
0.10
0.05
0.02
0.01
0.00
0
0.05
0.1
0.15
ω/ω_p

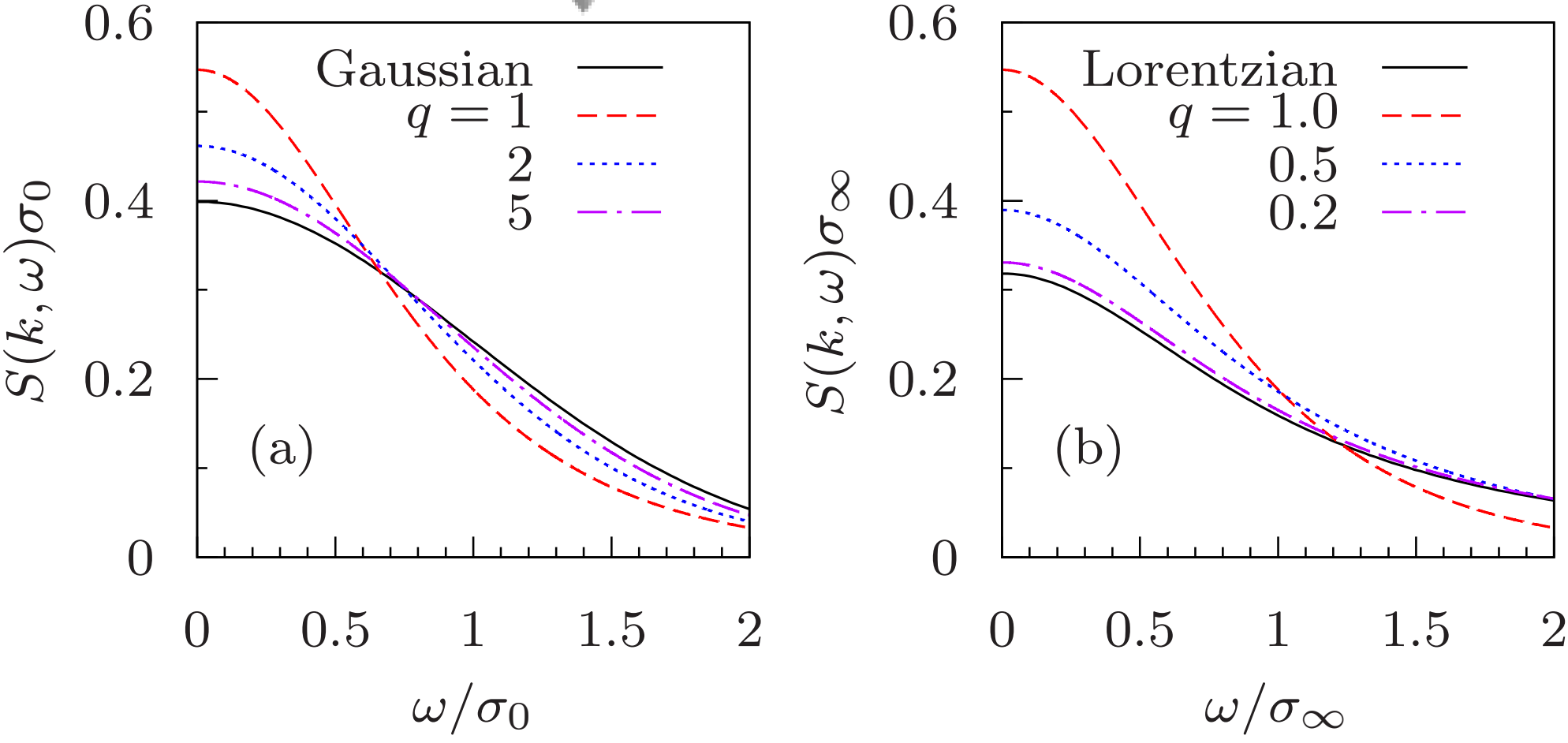
Gaussian
$q = 1$
2
5
(a)
$S(k,\omega)\sigma_0$
ω/σ_0
0
0.2
0.4
0.6
0
0.5
1
1.5
2
Lorentzian
$q = 1.0$
0.5
0.2
(b)
$S(k,\omega)\sigma_\infty$
ω/σ_∞

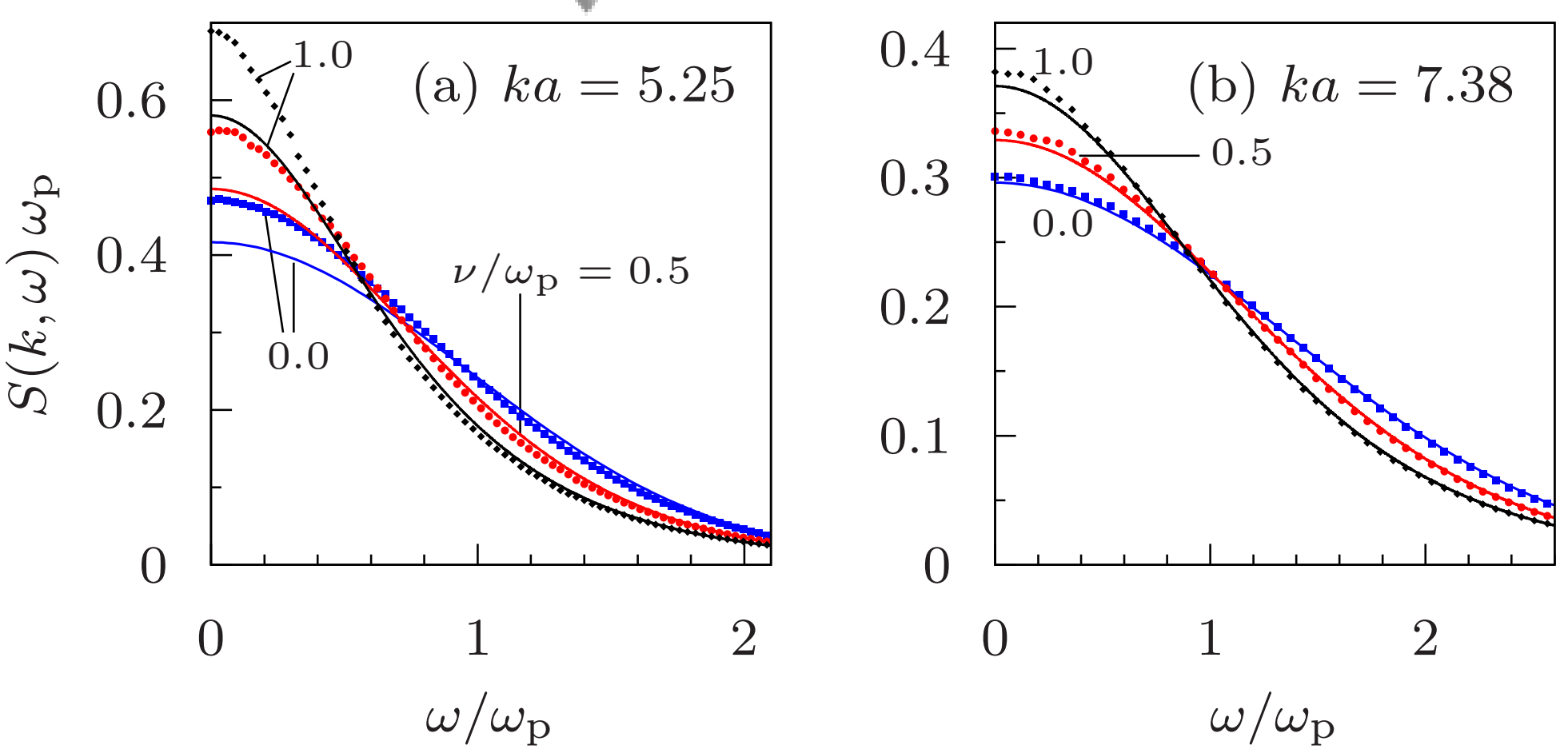
(a) $ka = 5.25$
(b) $ka = 7.38$
$S(k,\omega)\,\omega_\mathrm{p}$
ω/ω_p
$\nu/\omega_\mathrm{p} = 0.5$
1.0
0.5
0.0
0
0.2
0.4
0.6
0.1
0.3
1
2

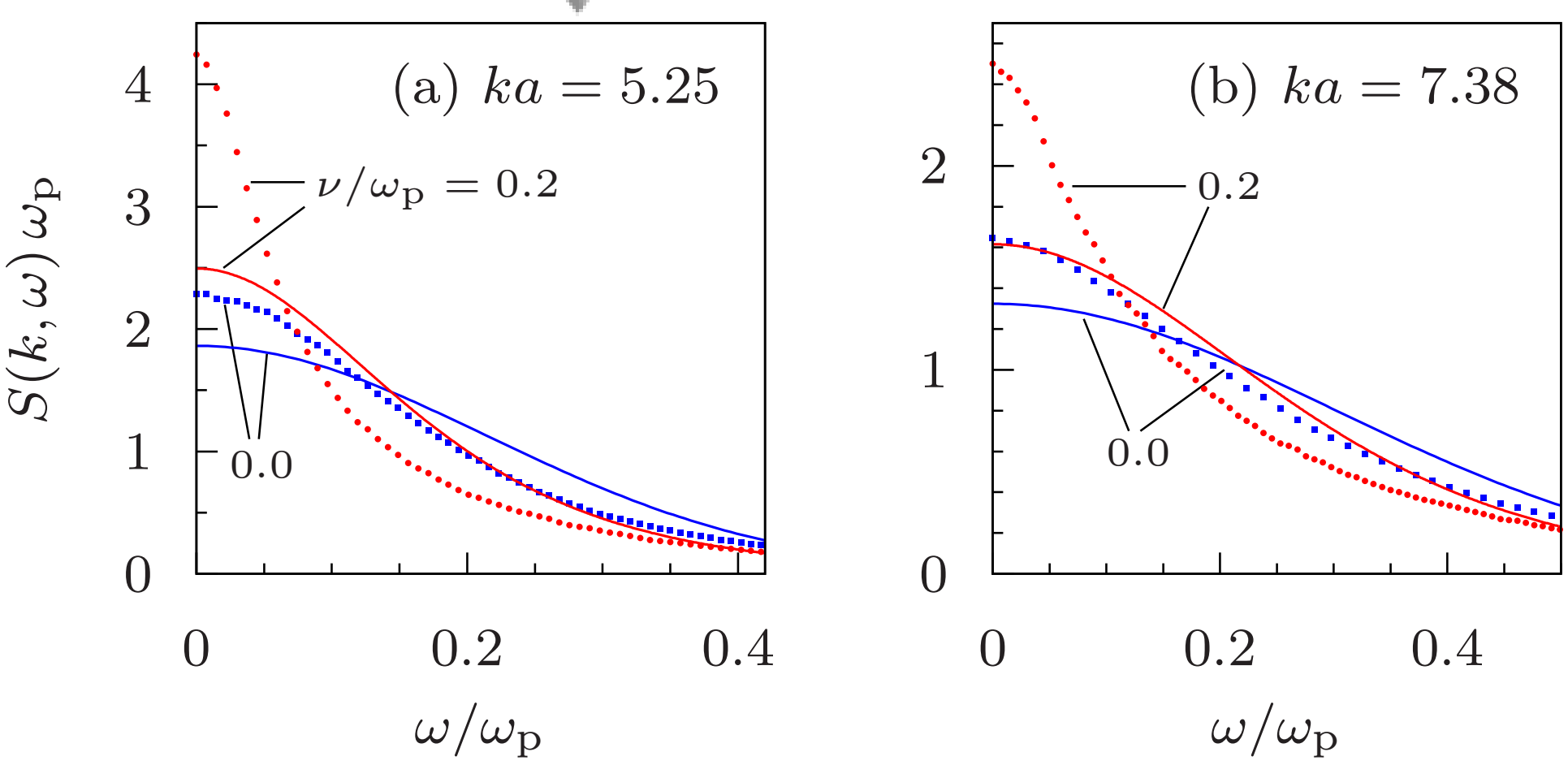
(a) $ka = 5.25$
(b) $ka = 7.38$
$\nu/\omega_{\rm p} = 0.2$
0.2
0.0
$S(k,\omega)\,\omega_{\rm p}$
$\omega/\omega_{\rm p}$
0
1
2
3
4
0.4